

Received February 1, 2022, accepted February 23, 2022, date of publication February 25, 2022, date of current version March 9, 2022.

Digital Object Identifier 10.1109/ACCESS.2022.3154784

5G-Compatible IF-Over-Fiber Transmission Using a Low-Cost SFP-Class Transceiver

MARCO A. FERNANDES^{1,2}, (Member, IEEE), BRUNO T. BRANDÃO^{1,2}, (Member, IEEE),
ABEL LORENCES-RIESGO¹, PAULO P. MONTEIRO^{1,2}, (Senior Member, IEEE),
AND FERNANDO P. GUIOMAR^{1,2}, (Member, IEEE)

¹Instituto de Telecomunicações, 3810-193 Aveiro, Portugal

²Department of Electronics, Telecommunications, and Informatics (DETI), University of Aveiro, 3810-193 Aveiro, Portugal

Corresponding author: Marco A. Fernandes (marcofernandes@av.it.pt)

This work was supported in part by the European Regional Development Fund (FEDER), through the Regional Operational Programme of Centre (CENTRO 2020) of the Portugal 2020 framework; and in part by the Financial Support National Public [Fundação para a Ciência e Tecnologia (FCT)] through Projects Optical Radio Convergence Infrastructure for Communications and Power Delivering (ORCIP) (CENTRO-01-0145-FEDER-022141), Utilização de Tecnologias de Reflectometria no melhoramento do futuro Internet das Coisas e Sistemas Ciber-Físicos (RETIOT) (Programa Operacional Competitividade e Internacionalização (POCI)-01-0145-FEDER-016432), LANDmaRk (POCI-01-0145-FEDER-031527), and OptWire (PTDC/EEI-TEL/2697/2021). The work of Marco A. Fernandes and Bruno T. Brandão was supported by the Ph.D. fellowships from FCT under Grant 2020.07521.BD and Grant 2021.05867.BD. The work of Fernando P. Guiomar was supported by the “la Caixa” Foundation (ID 100010434), under Grant LCF/BQ/PR20/11770015.

ABSTRACT With the rise of 5G and beyond, the ever-increasing data-rates demanded by mobile access are severely challenging the capacity of optical fronthaul networks. Despite its high reliability and ease of deployment, legacy digital radio-over-fiber (RoF) technologies face an upcoming bandwidth bottleneck in the short term. This has motivated a renewed interest in the development of analog RoF alternatives, owing to their high spectral efficiency. However, unlike its digital counterpart, analog RoF transmission requires a highly linear transceiver to guarantee signal fidelity. Typical solutions exploited in recent research works tend to adopt the use of bulky benchtop components, such as directly modulated lasers (DML) and photodiodes. Although this provides a convenient and quick path for proof-of-concept demonstrations, there is still a considerable gap between lab developments and commercial deployment. Most importantly, a key question arises: can analog-RoF transceivers meet the 5G requirements while being competitive in terms of cost and footprint? Following this challenge, in this work we exploit the use of a low-cost commercial off-the-shelf (COTS) small form-factor pluggable (SFP) transceiver, originally designed for digital transmission at 1 Gbps, which is properly adapted towards analog RoF transmission. Bypassing the digital electronics circuitry of the SFP, while keeping the original transmitter optical sub-assembly (TOSA) and receiver optical sub-assembly (ROSA), we demonstrate that high-performance 5G-compatible transmission can be performed by reusing the key built-in components of current low-cost SFP-class transceivers. Particularly, we demonstrate error vector magnitude (EVM) performances compatible with 5G 64QAM transmission both at 100 MHz and 400 MHz. Furthermore, employing a memory polynomial model for digital pre-distortion of the transmitted signal, we achieve 256QAM-compatible performance at 100 MHz bandwidth, after 20 km fronthaul transmission.

INDEX TERMS 5G, memory polynomial, analog radio-over-fiber.

I. INTRODUCTION

The imminent rise of 5G and beyond radio communications, together with the progressive adoption of the centralized radio-access network (C-RAN) architecture [1], is bringing new challenges for optical transceivers. Future transceivers will have to cope with very tight requirements in terms of

The associate editor coordinating the review of this manuscript and approving it for publication was Z. G. Zang¹.

bandwidth, latency and reliability [2]. Digital fronthauling based on the common radio public interface (CPRI) [3] specification has been adopted as the *de facto* standard for 4G-LTE signals, with its most recent version (eCPRI) dividing functionalities between the centralized unit and the distributed unit, thereby achieving improved latency and capacity [17]. However, for next generation RANs, this fronthaul architecture must be able to provide data rates beyond of hundred Gbps [4] due to the larger bandwidth of 5G signals and the use

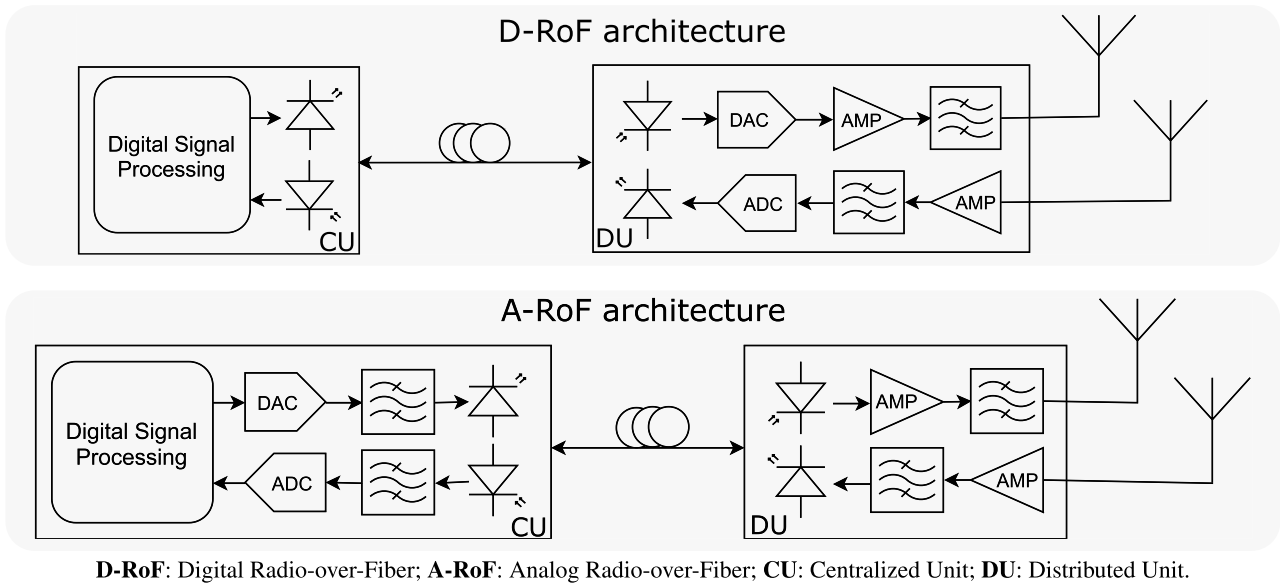


FIGURE 1. Schematic of two RAN concepts: i) employing D-RoF transmission (above), and ii) another depicting an A-RoF architecture (below).

of massive multiple input multiple output (MIMO) systems. This together with the tight latency requirements defined for 5G signals, has triggered research on whether analog fronthaul can be used instead [5]. Whereas analog fronthaul lacks the resilience of the digital counterpart, it does however reduce the requirements on the transceiver bandwidth and also minimizes the fronthaul latency [1].

The performance of analog radio-over-fiber (A-RoF) transceivers is impaired by several effects, including nonlinearities in the transceiver [6] and fiber dispersion, whose penalty can be enhanced by the laser chirp [7]. The presence of such undesired effects is enhanced when using low-cost transceivers, which are required for these applications. To mitigate fiber dispersion, the use of an intermediate frequency has been proposed for the mm-wave bands [8]. Mitigation of nonlinearities can be performed using several digital pre-distortion (DPD) techniques, such as memory polynomials [9], look-up-tables [10], or neural networks [11]. The complexity of these techniques should be taken into account, and therefore lower complexity solutions such as look-up-tables or memory polynomial are preferred.

Due to the widespread dissemination of digital communications, the main efforts from the industry rely on developing low-cost packaged digital transceivers, while most analog solutions remain based on costly discrete components, which require further driving/adaptation so that they can be used for research purposes. In this work, we address this scarcity of analog RoF solutions, exploiting a workaround to obtain low-cost analog transceivers through the adaptation of a commercial digital small form-factor pluggable (SFP) transceiver to support the analog transmission of 5G signals. We address key implementation issues such as the impact of crosstalk between transmitter and receiver ports, and then we proceed with experimentally testing the adapted low-cost transceiver

in an optical analog fronthaul. In order to maximize the transceiver performance, we propose a low-complexity DPD method based on a memory polynomial. We demonstrate that transmission over 20 km single-mode fiber (SMF) does not impose any major impairment on the signal quality, but nonlinear compensation is required to enable reception of a 256QAM signal with EVM below the 3.5% established limit [12].

In summary, the main novel contributions provided in this work can be enumerated as follows,

- i) proposal and demonstration of a simple adaption procedure over the electronic driving circuit of a low-cost digital SFP transceiver, enabling its compatibility with analog RoF transmission, while reusing the original packaging and TOSA / ROSA components;
- ii) detailed characterization of the adapted analog SFP transceiver at the component level (S-parameters) and system level (EVM performance in different 5G transmission scenarios);
- iii) performance enhancement of the adapted analog SFP transceiver using a low-complexity DPD model based on a memory polynomial;
- iv) experimental demonstration of the performance compatibility of the proposed analog SFP transceiver for the transmission of 5G signals with 100 MHz and 400 MHz with 64QAM modulated subcarriers, extended to 256QAM-compatible operation (100 MHz) enabled by a memory polynomial DPD.

II. ANALOG RADIO-OVER-FIBER FOR 5G ACCESS

Figure 1 depicts the concept of a typical RAN employing D-RoF transmission, and the alternative architecture with analog transmission. The first difference observed consists in the shift of equipment complexity from the distributed unit (DU) to the centralized unit (CU). This is mainly due

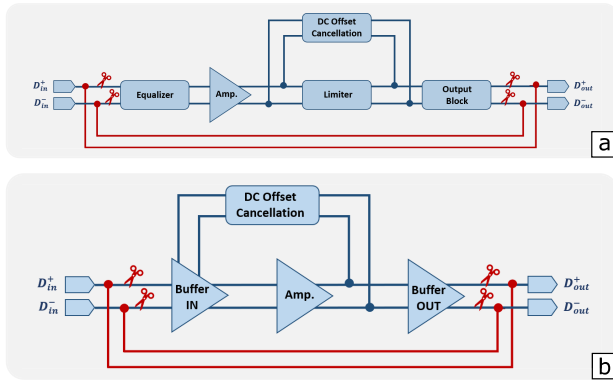


FIGURE 2. Simple adaptation to convert a commercial digital SFP into an analog RoF transceiver. Red lines represent the shunt wires soldered into the original PCB. (a) Modifications in the transmitter side and (b) in the receiver side.

to the digital-to-analog converter (DAC) and analog-to-digital converter (ADC) that were in the DU in the D-RoF scenario, performing A/D conversion in the uplink and D/A conversion in the downlink, which are relocated to the CU in the A-RoF case, performing D/A conversion in the downlink and A/D conversion in the uplink. This results in DUs that are simpler, cheaper and with lower power consumption.

Other main drivers for the adoption of A-RoF systems consist in their low-latency, ease of implementation and high-spectral efficiency. Since in the A-RoF scenario, the radio signals are directly transmitted, problems such as bandwidth multiplication are avoided. In typical D-RoF scenarios, this problem cannot be avoided, resulting in enormous data rates for 5G typical scenarios. In this scenario, considering the employment of CPRI (Option 8 / Split E), the data rate can be calculated using the following expression:

$$\text{data rate} = M \times S_r \times N \times 2 \frac{I}{Q} \times C_w \times C, \quad (1)$$

where M is the number of antennas per sector, S_r the sampling rate, N is the number of bits per sample, $2(I/Q)$ is a multiplication factor for in-phase (I) and quadrature-phase (Q) data, C_w is the factor of CPRI control word and C is a coding factor. From the expression analysis it is easy to conclude that for transmitting a given signal, the required fronthaul data rate will be significantly expanded. For instance, considering the case study of this paper, for the transmission of a 100 MHz signal, if we consider $M = 1$, $S_r = 1.5 \times 100$ MHz, $N = 15$, $C_w = 16/15$ and $C = 66/64$, the resulting data rate for the D-RoF scenario will be roughly 2.5 Gb/s. Considering the maximum bandwidth specified for 5G *i.e.* 16 aggregated components carriers (CCs) each with 400 MHz (total aggregated bandwidth of 6.4 GHz), the required data rate given by expression (1) with the aforementioned parameters is 158 Gbps, which would require the use of two high-end 100GBASE-LR4 transceivers (or even ER4-class, if the fronthaul is longer than 10 km), thus imposing a high cost and power consumption at the E/O ends and also a rather

inefficient use of the optical spectrum (4 wavelengths per transceiver). Instead, if A-RoF is considered, no bandwidth expansion is imposed, and the 6.4 GHz radio signal can be generated by an analog transceiver with a similar operating bandwidth, thereby reducing the cost of the electronic components and also reducing the spectral occupancy of the optical signal. A similar calculation for more than 100 antenna modules, a 4-sector device supporting 400 MHz baseband channels would roughly require 10 Tbps, which is equivalent to about 400 optical OOK-DSB-50GHz-grid channels [16]. These high-capacity examples clearly expose the critical upscaling issues that are associated with digital fronthauling, which is driving a renewed interest on the development of A-RoF solutions for 5G and beyond.

Another tight requirement for 5G networks is ultra low-latency communications, where this latency time can be reduced to 1 ms in urgent and specific scenarios. This is another advantage of A-RoF systems which have a significant gain in latency-terms when compared to its digital counterpart. All these advantages are increasing the interest of the scientific community in analog RANs, with multiple works highlighting these advantages in field-trials applications and real 5G networks [13]–[15]. Despite all the aforementioned advantages of analog transmission it is difficult to encounter a commercial off-the-shelf (COTS) analog optical transceiver. In the next section, we propose a simple procedure to take a COTS digital transceiver and convert it to perform analog transmission.

III. SFP ADAPTATION FOR ANALOG TRANSMISSION

The transceivers under test are COTS SFP transceivers designed for digital transmission at 1–10 Gb/s, which are nowadays ubiquitous in fiber-optic access networks, and whose cost is typically below 50 €. Let us start by unpacking the SFP transceiver and analyzing its key components. In Figure 3.a, we can identify three key parts of the digital SFP transceiver: i) the transmitter optical sub-assembly (TOSA), which performs electrical-to-optical (E/O) conversion using a directly-modulated laser, ii) the receiver optical sub-assembly (ROSA), which performs optical-to-electrical (O/E) conversion through an amplified photodiode, and iii) the printed circuit board (PCB) that is responsible for electrically driving the TOSA and ROSA components. Since these transceivers are designed for digital fiber communications, a set of necessary adaptations are required to enable the transmission of analog optical signals. Note, however, that the key optical transmission components, *i.e.* the TOSA and ROSA parts of the transceiver, are fundamentally responsible for the E/O and O/E conversion regardless of the properties of the transmitted/received signals, *i.e.* they are transparent to the type of transmission, and therefore can be kept in their original form, thus benefiting from the low-cost and small form-factor integration of these components. The main adaptations to enable analog transmission with the SFP transceiver are then required at the RF driving level in the PCB.

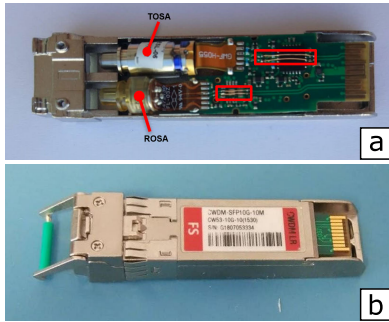


FIGURE 3. Final prototype of the converted analog RoF transceiver. (a) Open package showing the simple shunt modifications applied to the original SFP board and (b) analog RoF transceiver enclosed in the original SFP package.

A. ADAPTING THE ORIGINAL SFP ELECTRONICS FOR ANALOG TRANSMISSION

In order to preserve the original form-factor and pin-out of the standard SFP transceiver, we reuse the original digital board and perform a direct bypass of the digital electronics. Figure 2 shows a functional view of the modifications performed.

As evidenced in Figure 2, the modifications simply consist in bypassing the digital part of the board (buffering, equalization, amplification, DC offset cancellation and amplitude limitation) and directly wiring the input data pins to the output ones. The final physical layout of the modified transceiver can be observed in Figure 3, which evidences that these small modifications enable to obtain a low-cost analog RoF transceiver and keeping it in the original SFP package. Also note that, in this work, we have used a SFP evaluation board to provide access to the RF ports via SMA connectors.

IV. CHARACTERIZATION OF THE ANALOG SFP

Having successfully converted a digital transceiver into an analog one, we proceeded with the characterization of these transceivers. To this intent, firstly, S-parameter measurements were performed to characterize the frequency response of the analog transceivers. The E/O and O/E frequency response of the transmitter and receiver are illustrated in Figure 4. Note that the E/O frequency response of the TOSA is measured by using a calibrated photodiode at the receiver, while the corresponding O/E frequency response of the ROSA is obtained after de-embedding the frequency response of the TOSA. From Figure 4a we see that the transmitter shows a considerable conversion loss of 40 dB on average for frequencies up to 3 GHz and beyond 3 GHz the loss increases gradually, exceeding 55 dB at 10 GHz. This shows the already known poor conversion efficiency of direct modulated lasers. For the receiver it can be seen that the O/E conversion gain shows a decreasing trend from 45 dB near DC, down to 40 dB at 7 GHz. After 7 GHz, the performance degrades severely. When observing the combined response of the transmitter and the receiver, (Figure 4b) we see that for frequencies below 3 GHz there is a gain in the system, provided by the receiver TIA. However, when increasing the frequency for

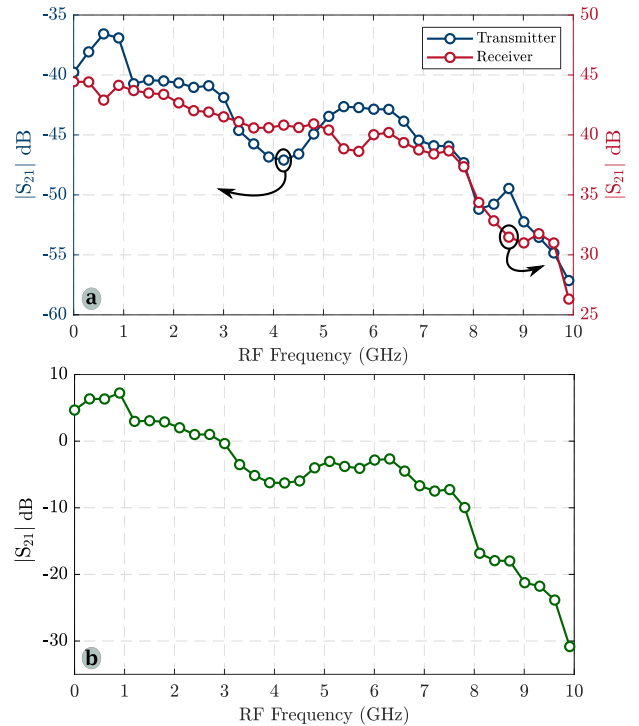


FIGURE 4. (a) Transmitter and receiver E/O and O/E frequency responses respectively. (b) Combined $|S_{21}|$ of the transmitter and receiver.

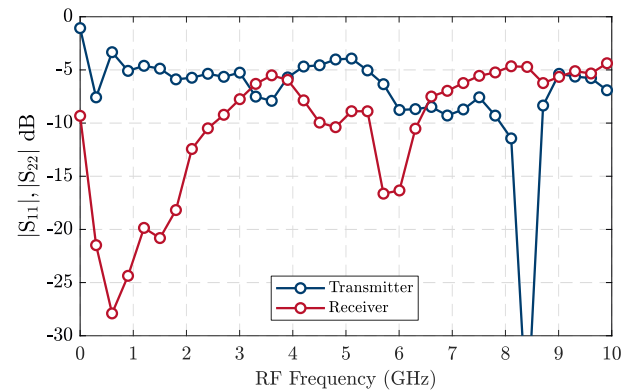


FIGURE 5. Electrical S_{11} and S_{22} responses of the transmitter and receiver respectively.

values above 7.5 GHz the system insertion loss becomes too high to apply in a practical scenario. The results of the impedance matching measurement at the transmitter and receiver RF ports are shown in Figure 5. The input reflection coefficient at the transmitter input RF port ($|S_{11}|$) show a bad impedance matching with the $|S_{11}|$ being mostly between -4 dB and -8 dB in the frequency range tested. In contrast, the receiver results reveal two regions with good port impedance matching, with $|S_{22}|$ equal or below -10 dB. The first one is from DC up to 2.5 GHz and the second one is from 5.5 GHz up to 6.5 GHz. The clear dip below -30 dB in the $|S_{11}|$ of the transmitter can be attributed to a resonance in the input circuit confined between 8 GHz and 9 GHz. Overall, this S-parameter characterization shows the

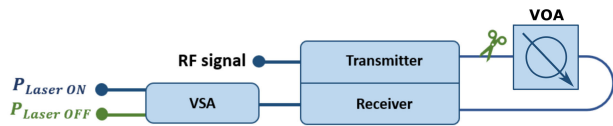


FIGURE 6. Diagram of the setup used to measure the transceiver crosstalk.

major impact of the transmitter conversion loss in the system. It is worth noting that this simple digital-to-analog adaptation procedure, basically consisting of four bypass wires, has been performed with the main aim of providing a proof-of-concept and easily reproducible demonstration. However, it should be noted that improved impedance matching and conversion efficiency might be achievable if the original SFP digital electronics are entirely replaced by an analog driving board, at the expense of a longer development time. Nevertheless, the premise of this work is to assess the performance limits of such a simple and fast digital-to-analog SFP conversion procedure.

A. CROSSTALK MEASUREMENTS

Crosstalk between the transmitter and receiver can be a performance bottleneck in A-RoF systems. Addressing this subject, we advanced the characterization process by measuring the crosstalk in our A-RoF transceiver. In order to quantify the impact of this problem in further tests, we designed a simple experiment consisting in measuring the received RF power with the laser on and off. The setup used to measure the crosstalk is depicted in Figure 6. If the transmitter and receiver are disconnected, it is not expected to receive any RF power, however, this power still has a significant value due to the crosstalk.

We have defined crosstalk as the ratio between the power received with the laser off and the one with laser on:

$$\Delta P = \frac{P_{Laser\ OFF}}{P_{Laser\ ON}} \tag{2}$$

Fixing the RF power to 0 dBm, we measured the value of ΔP sweeping the RF frequency between 1 GHz and 10 GHz. These results are presented in Figure 7, which shows a clear dependency between the crosstalk and the RF carrier frequency. For higher frequencies (above 8 GHz), the crosstalk is so high, that the RF received power is the same, regardless of whether the optical link is connected or disconnected.

Given the EVM-SNR relationship,

$$EVM (\%) = 10^{-\frac{SNR}{20}} \times 100, \tag{3}$$

if we assume all the crosstalk to be noise, we can measure the impact that it will have on the EVM. Since we are aiming to transmit 5G signals over an RF carrier of 3.5 GHz, the EVM will always have a floor limit of 10%, which already does not comply with the 3GPP requirements for modulations formats of 256QAM and 64QAM [12]. These results render the joint utilization of the transmitter and receiver in the transceiver more challenging, degrading the overall transmission performance. To overcome this problem and to ensure that the

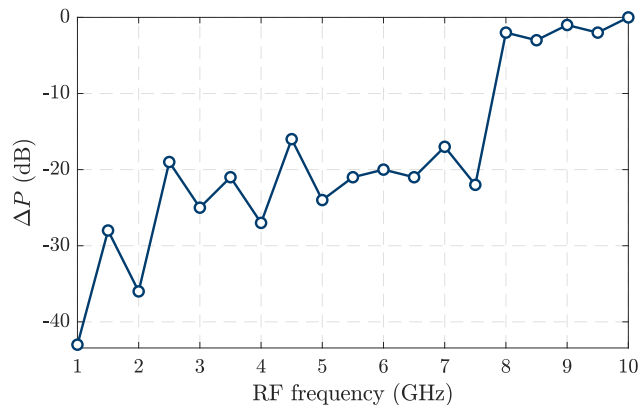


FIGURE 7. Dependency of the crosstalk with the RF frequency with 0 dBm RF power at the transmitter.

transceiver crosstalk is avoided, in all of the remaining tests we have decided to use TOSA and ROSA from different SFPs packages. Although this choice implies some hardware inefficiency (one TOSA/ROSA is unutilized per SFP pair), it guarantees a crosstalk-free operation.

V. EXPERIMENTAL SETUP

In order to emulate a real analog optical fronthaul, we have implemented the experimental setup shown in Figure 8. The setup is composed of an Arbitrary Waveform Generator (AWG) responsible for the generation of the RF baseband signal. This AWG has two differential output channels corresponding to the I and Q waveforms. This signal is then up-converted by the IQ mixer to an RF carrier of 3.5 GHz, corresponding to the standardized FR1 [2], before directly modulating the analog optical transmitter. The optical signal then travels through a given length of Single Mode Fiber (SMF). Before the optical receiver, there is a Variable Optical Attenuator (VOA), which enables the control of the optical power at the photodiode. The optical receiver performs the O/E conversion and this electrical signal is received in the Vector Signal Analyzer (VSA). The VSA down-converts the signal and demodulates it using standard compensation algorithms.

In order to maximize the performance of the low-cost transceivers, we propose the use of nonlinear DPD based on the following memory polynomial model,

$$z(n) = \sum_{k=0}^{K-1} \sum_{q=0}^{Q-1} a_{kq} \cdot y(n-q) \cdot |y(n-q)|^k, \tag{4}$$

where y is the transmitted signal without pre-distortion, z is the pre-distorted signal, K is the nonlinear order and Q is the memory depth. The optimization of the memory polynomial coefficients, a_{kq} , follows the strategy described in Figure 8. First, the signals are generated in the AWG without DPD. The measured signals are then used to calculate the coefficients of the memory polynomial by comparison with the transmitted

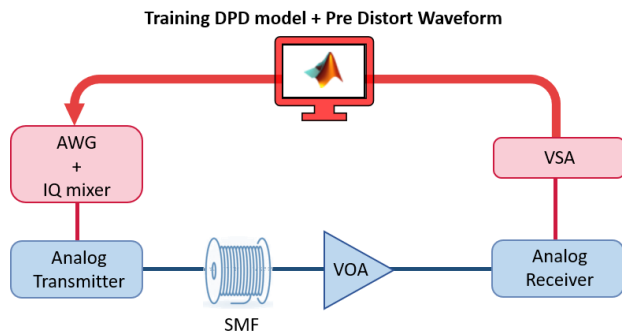


FIGURE 8. Experimental setup for extracting and applying a DPD model in a low-cost optical fronthaul.

waveform. After calculating the coefficients, the signal is pre-distorted with the DPD model.

The experimental analysis is divided in the following stages: i) back-to-back (B2B) performance assessment of the TOSA/ROSA transceiver pair, ii) fronthaul performance assessment, in which we consider a fiber link composed of 20 km SMF, and iii) A-RoF performance enhancement.

VI. EXPERIMENTAL 5G RESULTS

A. 5G FR1 TRANSMISSION

1) OPTICAL B2B

The first test consisted in analyzing the performance of the fronthaul in a simple scenario without optical fiber. The VOA was used to set the optical power into the photodiode to -12 dBm. This test consisted in optimizing the RF power for the 256QAM 5G signal. These optimizations were done for various DPD models varying the values of K and Q described in equation (4). The first implemented model consists only of a linear compensation with one sample memory. After, we tested a DPD model without memory ($Q = 1$), while increasing the nonlinear order of the model (K) until obtaining the best performance. With the optimized value of K , we increased the memory of the model until finding its best value. The obtained results are plotted in Figure 9. As can be seen, without DPD the best EVM was obtained for an RF power of 0 dBm, and has a value of 4.3%. Note that this value is above the 3.5% limit established by 3GPP for 256QAM transmission. The linear compensation corresponding to the blue dashed line in the figure presented similar results to those obtained without DPD. With all the nonlinear models implemented we obtained a considerable EVM reduction, with the best DPD model ($Q = 1, K = 5$), yielding an EVM of 3.2%. This model shows also to be better in terms of RF power margin where the EVM is below 3.5%, providing approximately a 2 dB tolerance for transmitted power detuning. Not shown here for brevity but increasing the nonlinear order for values higher than 5 resulted in a progressive loss of performance, likely triggered by a less accurate model extraction of higher-order nonlinearities. It is interesting to observe that the best absolute performance was obtained for a higher power than the optimum without DPD (3 dBm),

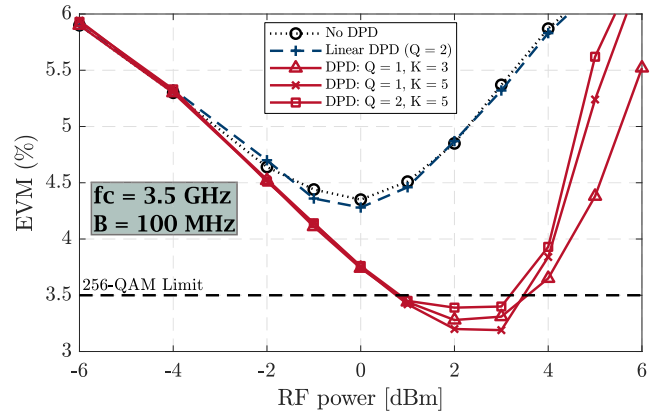


FIGURE 9. Measured EVM in B2B for the cases of no DPD, linear DPD and different nonlinear DPD based on memory polynomials, for a 100 MHz signal with a 3.5 GHz carrier.

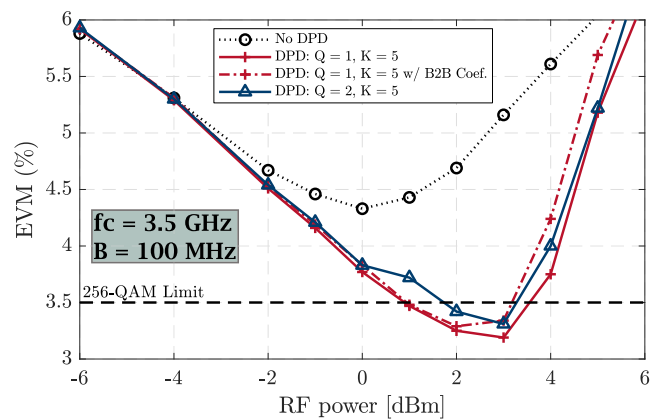


FIGURE 10. Measured EVM after 20 km SMF for the cases of no DPD and different nonlinear DPD based on memory polynomials, for a 100 MHz signal with a 3.5 GHz carrier.

which is a well-known advantage of nonlinear compensation in general: by mitigating nonlinearities, higher powers can be launched into the transmission system, thereby resulting in an improved SNR and/or power-budget. It is worth noticing that, all the considered DPD models in Figure 9 enable to successfully transmit a 5G 256QAM signal with an EVM below the 3GPP limit.

2) 20 km ANALYSIS

After studying the B2B performance, we added 20 km of SMF in order to get a more realistic fronthaul scenario. With this setup, there were two main goals. First, to verify if the model obtained in B2B is accurate enough to achieve the best transmission performance with a fiber fronthaul. This would bring a great advantage in practical terms, enabling the optimization of the DPD model for the optical transceivers in a controlled laboratory environment without requiring individual optimization in different fronthaul networks. The other main goal of this test, which is also inherently related with the first, is to test whether a long fronthaul link composed of 20 km SMF would introduce memory effects in the system.

With these goals in mind, we have continued the tests using the best DPD model obtained in B2B ($Q = 1, K = 5$) and with $Q = 2$ and $K = 5$. For the memoryless model ($Q = 1, K = 5$), we have measured the performance applying the model obtained in B2B as well as extracting a new model taking into account the 20 km in the system. It is worth noticing that the insertion of the fiber link required to increase the power in the photodiode to -10.5 dBm in order to achieve the best performance. The obtained results are shown in Figure 10. Without DPD the performance remains similar to the B2B case, with minimum EVM of 4.3% when the RF power is 0 dBm. Through the analysis of Figure 10, it is possible to conclude that the model obtained in B2B is still valid up to an RF power of 2 dBm, achieving a minimum EVM of 3.3%. The benefits of extracting the model again are visible for higher powers, enabling to achieve an EVM of 3.2% for an RF power of 3 dBm. It is worth to notice that the model obtained in B2B was still capable of presenting a very good performance being only 0.1% worse than those obtained with 20 km fiber link. The next step was to analyze if the 20 km SMF introduced memory in the system, so we extracted and applied a memory polynomial with $Q = 2$ and $K = 5$, which is signaled in the figure by a blue solid line. The system remains memoryless since the performance degrades relatively to the $Q = 1, K = 5$ scenario, yielding a minimum EVM of 3.3% at the optimum RF power of 3 dBm. Once again with all the DPD models, it was possible to obtain an EVM below the 3GPP limit for 256QAM.

Considering equation (3) we can calculate the SNR gain obtained with DPD. An EVM of 4.3% corresponds to an SNR of 27.3 dB, whereas an EVM of 3.2% corresponds to an SNR of 29.9 dB. Therefore, we may conclude that DPD effectively provides an SNR improvement of approximately 3 dB, which is a remarkable gain. These improvements are clear when observing the spectrum of the signal with and without pre-distortion. In Figure 11 it is possible to observe the improvement on the signal spectrum at the power of 3 dBm caused by the usage of DPD. Without DPD there is a clear nonlinear phenomenon in the adjacent bands of the signal, which is commonly designated as “spectral regrowth”. It is possible to see that the applied DPD model compensates almost completely for these bands. The signal spectra obtained at the optimum power without DPD (0 dBm) is also shown in Figure 11. From the results, we may conclude that DPD has effectively compensated for the nonlinear distortions generated by the 3 dB increased power, thus resulting in an effective gain of 3 dB in SNR, which very nearly matches the observed gains in terms of EVM.

B. 5G FR2 TRANSMISSION

1) IF ANALYSIS

Since 3GPP has defined the mmWave range for FR2 transmission, to be able to transmit these signals with our adapted transceivers, we need to convert them to an intermediate frequency (IF), leading to a system configuration that is typi-

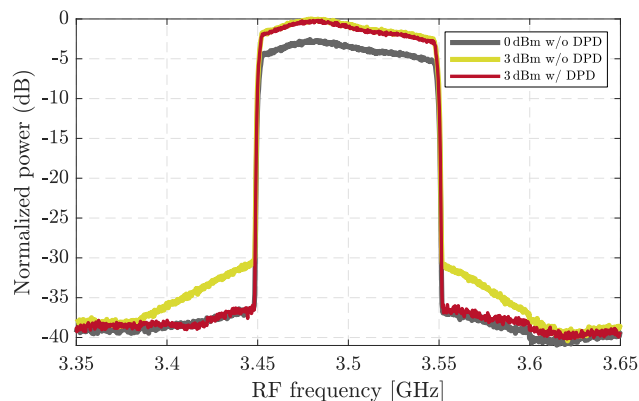


FIGURE 11. Measured spectra for the optical case without DPD (0 dBm), and for the optical case when performing DPD (3 dBm) before and after applying the model.

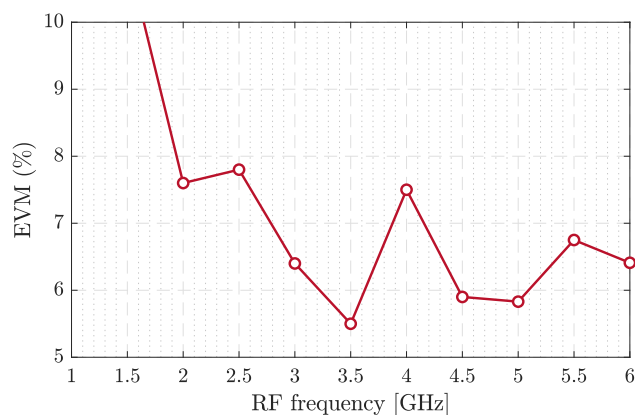


FIGURE 12. Measured EVM for different IF values with a 64QAM 400 MHz transmitted signal.

cally designated as IF-over-fiber (IFoF). To optimize the best suited IF for our system, we started by sending a 400 MHz 64QAM signal using different IFs with an RF power of 0 dBm and analysed the measured EVM. The results obtained from this analysis are depicted in Figure 12. Despite not showing a clear tendency, the results show an EVM minimum of 5.5% for an IF of 3.5 GHz. Besides maximizing the A-RoF transceiver performance, this 3.5 GHz IF choice also shows the advantage of enabling an improved compatibility between the FR1 and FR2 transmission modes.

2) PERFORMANCE ASSESSMENT

After optimizing the value of the transmitted IF we measured the performance achievable in an FR2 scenario with our setup. To this intent, we used the same 5G signal as before (64QAM, 400 MHz) at the optimum IF of 3.5 GHz. With this signal, we performed tests without fiber and with 20 km SMF. Figure 13 shows the results obtained when sweeping the RF power transmitted, without any DPD and with the best DPD model found ($Q = 2, K = 3$), for each scenario. It is observable from the presented results that there is a slight increase in the optimum RF power, which is related with having

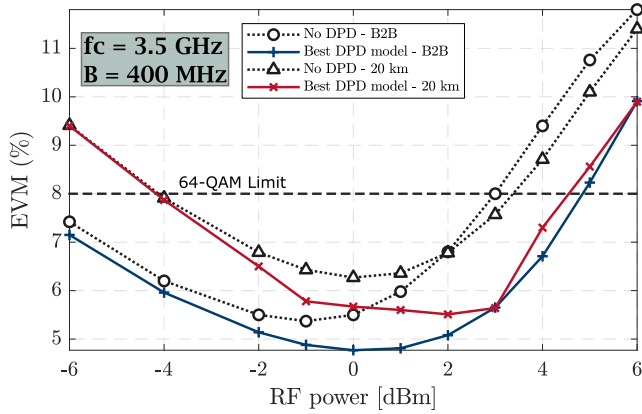


FIGURE 13. Measured EVM in an OB2B scenario and with 20 km SMF, for the cases of no DPD and best DPD model obtained ($Q = 2, K = 3$), for a 400 MHz signal with a 3.5 GHz carrier.

increased the signal bandwidth from 100 MHz to 400 MHz, leading to a power spreading over the frequencies spectrum. This bandwidth increase also leads to the enhancement of filtering effects that introduce more memory into the system, resulting in an optimum DPD model with a memory tap. From the results, we observe that, for both scenarios, simply optimizing the RF power driving the SFP is enough to achieve 64QAM transmission (where the 3GPP limit is 8% EVM). Without any DPD we obtained an EVM of 5.2% and 6.3%, in OB2B and with 20 km SMF, respectively. However, with the best DPD models found, the performance was improved to 4.8% in the OB2B scenario, and 5.5% with 20 km SMF.

C. DPD COMPLEXITY ANALYSIS

An underlying problem with introducing advanced techniques for nonlinear DPD is the increased complexity in these systems. For this reason, we decided to perform a complexity analysis of the proposed memory polynomial DPD method. In order to quantify their complexity, we will use the number

of real multiplications (N_{RMs}) required to pre-distort each sample of the transmitted signal. To proceed with this analysis, let us return to equation (4) and, since both a_{kq} and $y(n)$ are complex numbers, rewrite it as,

$$z(n) = \sum_{k=0}^{K-1} \sum_{q=0}^{Q-1} \underbrace{([a_{kq,r}y_r(n-q) - a_{kq,i}y_i(n-q)])}_{\text{Real component (2 RMs)}} + j \underbrace{[a_{kq,r}y_i(n-q) + a_{kq,i}y_r(n-q)]}_{\text{Imaginary component (2 RMs)}} |y(n-q)|^k, \tag{5}$$

where we consider that the absolute value of $y(n-q)$ can be computed as,¹

$$|y(n-q)| = \sqrt{\underbrace{y_r(n-q)^2 + y_i(n-q)^2}_{2 \text{ RMs}}}. \tag{6}$$

Noting that the number of RMs grows linearly with the DPD memory, Q , we can start by analyzing the model complexity for the case of $Q = 1$, with increasing polynomial order, K , as shown in equations (8) to (11), as shown at the bottom of the page.

Note that, when computing $|y(n)|^k$ for $k > 1$, we assume that the value of $|y(n)|^{k-1}$ has already been previously computed and stored in memory, and therefore there is only one extra real multiplication needed to evaluate $|y(n)|^k = |y(n)|^{k-1}|y(n)|$.

Finally, generalizing the above examples for any value of K and Q , we obtain that the following analytical expression

¹Note that, for simplicity, we neglect the complexity associated with the $\sqrt{\cdot}$ operation, as its hardware implementation might follow different algorithms, namely resorting to the use of look-up tables. Nevertheless, it is worth noting that for any memory polynomial of order $K > 1$ and memory Q , only Q square-root operations are actually required; i.e. once the value of $|y(n-q)|$ is first computed, it can be stored in memory for the subsequent evaluation of its $|y(n-q)|^k$ products.

- $K = 1$:

$$\underbrace{([a_{00,r}y_r(n) - a_{00,i}y_i(n)])}_{2 \text{ RMs}} + j \underbrace{[a_{00,r}y_i(n) + a_{00,i}y_r(n)]}_{2 \text{ RMs}} \underbrace{|y(n)|^0}_{=1} \rightarrow 4 \text{ RMs} \tag{8}$$

- $K = 2$:

$$\underbrace{[a_{10,r}y_r(n) - a_{10,i}y_i(n)]|y(n)|}_{3 \text{ RMs}} + j \underbrace{[a_{10,r}y_i(n) + a_{10,i}y_r(n)]|y(n)|}_{3 \text{ RMs}} \xrightarrow{+2 \text{ from eq. (6)} + 4 \text{ from eq. (8)}} 12 \text{ RMs} \tag{9}$$

- $K = 3$:

$$\underbrace{[a_{20,r}y_r(n) - a_{20,i}y_i(n)]|y(n)|^2}_{3 \text{ RMs}} + j \underbrace{[a_{20,r}y_i(n) + a_{20,i}y_r(n)]|y(n)|^2}_{3 \text{ RMs}} \xrightarrow{+12 \text{ from eq. (9)} + 1 \text{ from } |y(n)|^2} 19 \text{ RMs} \tag{10}$$

- $K = 4$:

$$\underbrace{[a_{30,r}y_r(n) - a_{30,i}y_i(n)]|y(n)|^3}_{3 \text{ RMs}} + j \underbrace{[a_{30,r}y_i(n) + a_{30,i}y_r(n)]|y(n)|^3}_{3 \text{ RMs}} \xrightarrow{+19 \text{ from eq. (10)} + 1 \text{ from } |y(n)|^3} 26 \text{ RMs} \tag{11}$$

that fully describes the complexity (in number of RMs) of the memory polynomial model,

$$N_{\text{mul}} = \begin{cases} 4Q, & \text{if } K = 1, \\ (6 + 6(K - 1) + (K - 2))Q, & \text{if } K \geq 2. \end{cases} \quad (7)$$

Having obtained this relation, we can now calculate the number of multiplications required to implement the memory polynomial DPD at the best complexity-vs-performance tradeoff previously found in Figs. 9, 10 and 13, i.e. $K = 5$, $Q = 1$ and $K = 3$, $Q = 2$, yielding a complexity of 33 and 38 multiplications, respectively. Through this in-depth complexity analysis, we can then conclude that the utilized memory polynomial model is effectively a low-complexity subsystem. As a baseline for comparison, the number of multiplications required for its operation is lower than what would be required for a standard linear filter with 10 taps (i.e. $4Q$ as in the upper branch of (8), for $K = 1$).

VII. CONCLUSION

In this paper, we addressed one of the main challenges in the upcoming next-generation RANs, namely, the bandwidth bottleneck imposed by digital fronthauling in typical architectures. With the rise of 5G and the emergence of 6G specifications, it is required to search for alternative technologies that meet these unprecedented demands. Answering to these requirements and responding to the scarcity of low-cost analog optical transceivers, we have demonstrated a simple procedure to take a low-cost COTS digital SPF transceiver, and modify it to perform analog transmission. With the simple modifications exposed in the paper, we were able to obtain an SFP-packaged analog transceiver, capable of transmitting 100 MHz and 400 MHz 64QAM signals meeting the 3GPP EVM requirements. Moreover, a memory-polynomial based pre-distortion technique has been shown to partially counteract the limitations inherent to the simple digital-to-analog adaption procedure, enabling to meet the EVM specifications for transmitting a 100 MHz 256QAM signal over 20 km SMF.

Although the proposed digital-to-analog adaption of the SFP transceiver is not deemed as a practical solution for the marketization of analog RoF transceivers, the results presented in this work demonstrate that it is possible to design high-performance analog RoF solutions using low-cost components that have found matured deployment in the low-end digital optics market. Furthermore, the analog-adaption methodology and digital pre-distortion technique demonstrated in this work might provide useful insights for the research community, facilitating the access to low-cost RoF solutions as an enabling technology to support the experimentation and prototyping of complex 5G and 6G optical access architectures in laboratory environments.

REFERENCES

- [1] I. A. Alimi, A. L. Teixeira, and P. P. Monteiro, "Toward an efficient C-RAN optical fronthaul for the future networks: A tutorial on technologies, requirements, challenges, and solutions," *IEEE Commun. Surveys Tuts.*, vol. 20, no. 1, pp. 708–769, 1st Quart., 2018, doi: 10.1109/COMST.2017.2773462.

- [2] *Technical Specification Group Services and System Aspects: Release 15 Description*, Standard 3GPP TR 21.915, 2019.
- [3] *Common Public Radio Interface (CPRI); Interface Specification*, document CPRI Specification V7.0, 2015.
- [4] *Technical Specification Group Radio Access Network: Study on CU-DU Lower Layer Split for NR, Annex A: Fronthaul Bandwidth (Release 15)*, Standard 3GPP TR 38.816, 2017.
- [5] C. Ranaweera, E. Wong, A. Nirmalathas, C. Jayasundara, and C. Lim, "5G C-RAN with optical fronthaul: An analysis from a deployment perspective," *J. Lightw. Technol.*, vol. 36, no. 11, pp. 2059–2068, Jun. 1, 2018, doi: 10.1109/JLT.2017.2782822.
- [6] J. Wang, C. Liu, J. Zhang, M. Zhu, M. Xu, F. Lu, L. Cheng, and G.-K. Chang, "Nonlinear inter-band subcarrier intermodulations of multi-RAT OFDM wireless services in 5G heterogeneous mobile fronthaul networks," *J. Lightw. Technol.*, vol. 34, no. 17, pp. 4089–4103, Sep. 1, 2016, doi: 10.1109/JLT.2016.2584621.
- [7] B. G. Kim, S. H. Bae, H. Kim, and Y. C. Chung, "RoF-based mobile fronthaul networks implemented by using DML and EML for 5G wireless communication systems," *J. Lightw. Technol.*, vol. 36, no. 14, pp. 2874–2881, Jul. 15, 2018, doi: 10.1109/JLT.2018.2808294.
- [8] S.-H. Cho, H. Park, H. S. Chung, K. H. Doo, S. Lee, and J. H. Lee, "Cost-effective next generation mobile fronthaul architecture with multi-IF carrier transmission scheme," in *Proc. Opt. Fiber Commun. Conf.*, Mar. 2014, pp. 1–3.
- [9] J. Zhang, J. Wang, M. Xu, F. Lu, L. Chen, J. Yu, and G.-K. Chang, "Memory-polynomial digital pre-distortion for linearity improvement of directly-modulated multi-IF-over-fiber LTE mobile fronthaul," in *Proc. Opt. Fiber Commun. Conf.*, Mar. 2016, pp. 1–3.
- [10] X. N. Fernando and A. B. Sesay, "Look-up table based adaptive predistortion for dynamic range enhancement in a radio over fiber link," in *Proc. IEEE Pacific Rim Conf. Commun., Comput. Signal Process. (PACRIM) Conf.*, Aug. 1999, pp. 26–29, doi: 10.1109/PACRIM.1999.799469.
- [11] S. Liu, M. Xu, J. Wang, F. Lu, W. Zhang, H. Tian, and G.-K. Chang, "A multilevel artificial neural network nonlinear equalizer for millimeter-wave mobile fronthaul systems," *J. Lightw. Technol.*, vol. 35, no. 20, pp. 4406–4417, Oct. 15, 2017, doi: 10.1109/JLT.2017.2717778.
- [12] *User Equipment (UE) Radio Transmission and Reception; Part 1: Range 1 Standalone (Release 15)*, Standard 3GPP TS 38.101-1, 2018.
- [13] M. A. Fernandes, P. A. Loureiro, B. T. Brandao, A. Lorences-Riesgo, F. P. Guiomar, and P. P. Monteiro, "Multi-carrier 5G-compliant DML-based transmission enhanced by bit and power loading," *IEEE Photon. Technol. Lett.*, vol. 32, no. 12, pp. 737–740, Jun. 15, 2020, doi: 10.1109/LPT.2020.2994045.
- [14] A. Mufutau, F. Guiomar, M. Fernandes, A. Lorences-Riesgo, A. Oliveira, and P. Monteiro, "Demonstration of a hybrid optical fiber-wireless 5G fronthaul coexisting with end-to-end 4G networks," *J. Opt. Commun. Netw.*, vol. 12, pp. 72–78, Mar. 2020.
- [15] M. Alzenad, M. Z. Shakir, H. Yanikomeroğlu, and M.-S. Alouini, "FSO-based vertical backhaul/fronthaul framework for 5G+ wireless networks," *IEEE Commun. Mag.*, vol. 56, no. 1, pp. 218–224, Jan. 2018.
- [16] Z. Zakrzewski, "D-RoF and A-RoF interfaces in an all-optical fronthaul of 5G mobile systems," *Appl. Sci.*, vol. 10, no. 4, p. 1212, Feb. 2020.
- [17] *Common Public Radio Interface Interface Specification*, document eCPRI Interface Specification V1.0, 2017.



MARCO A. FERNANDES (Member, IEEE) received the M.Sc. degree in electronics and telecommunications engineering from the University of Aveiro, in 2019. He is currently pursuing the Ph.D. degree in MAP-tele doctorate program from the University of Aveiro, the University of Porto, and the University of Minho. During his M.Sc. degree, he has worked with analog-radio over fiber applied to 5G communications. During his master's, he worked with advanced

radio-over-fiber transmission providing 5G-solutions for Optical Radio Convergence Infrastructure for Communications and Power Delivering (ORCIP-www.orcip.pt) testbed. He is currently participates in multiple research projects, mainly involved high-capacity free space optics (FSO) transmission and machine learning applications. He has authored or coauthored more than 15 scientific publications in leading international journals and conferences. He is an Optica Member. He received the Ph.D. Grant from FCT, in 2020. In 2021, he was a finalist in OFC2021 Corning Student Award.



BRUNO T. BRANDÃO (Member, IEEE) received the M.Sc. degree in electronics and telecommunications engineering from the University of Aveiro, Portugal, in 2019. During his M.Sc. degree, he has developed an analogue radio-over-fibre link, based on low-cost optical transceivers, for 4G and 5G communication support. Since 2019, he has been with the Telecommunications Ph.D. Program (MAP-Tele), a joint venture between the Universities of Minho, Portugal, and the Universities of Aveiro. In his Ph.D. studies, he is developing and implementing digital signal processing algorithms in reconfigurable hardware for real-time coherent communication systems. Along with the Ph.D. studies, he is working in the RETIOT Project under the M.Sc. fellowship in which he is developing a distributed radio system for both radio communications and coherent radar applications. He also designed an RF frontend to serve as an interface between the remote user equipment and the radio-over-fibre link. This work was done under the scope of ORCIP infrastructure (www.orcip.pt) at the Instituto de Telecomunicações.



ABEL LORENCES-RIESGO received the Ph.D. degree from the Chalmers University of Technology, in 2017. From 2017 to 2019, he worked as a Postdoctoral Researcher at Telecomunicações-Aveiro. In 2019, he joined the Optical Communication Technology Laboratory, Paris Research Center, Huawei Technologies France, as a Senior Engineer. He has authored or coauthored more than 70 papers in leading international journals and conferences. His main research interests include fiber optic communications and digital signal processing.



PAULO P. MONTEIRO (Senior Member, IEEE) is currently an Associate Professor at the University of Aveiro and a Senior Researcher at the Instituto de Telecomunicações, where he is also a Research Coordinator of optical communication systems (<https://www.it.pt/Groups/Index/59>). He successfully tutored over 14 Ph.D. students and 24 master's students. He has participated in more than 26 research projects. He has authored/coauthored more than 18 patent applications, over 115 articles in journals, and 380 conference contributions. His main research interests include optical communications and reflectometry systems.



FERNANDO P. GUIOMAR (Member, IEEE) received the M.Sc. and Ph.D. degrees in electronics and telecommunications engineering from the University of Aveiro, Portugal, in 2009 and 2015, respectively. Since 2017, he has been a Senior Researcher at the Instituto de Telecomunicações, Aveiro, where his main research interests are focused within the area of fiber-based and free-space optical communication systems, including the development of digital signal processing algorithms, advanced modulation and coding, constellation shaping and non-linear modeling and mitigation. He has authored or coauthored more than 100 scientific publications in leading international journals and conferences. He is an OSA Member. In 2015, he received a Marie Skłodowska-Curie individual fellowship, jointly hosted by the Politecnico di Torino, Italy, and CISCO Optical GmbH, Germany. In 2016, he has received the Photonics21 Student Innovation Award, distinguishing industrial-oriented research with high impact in Europe. In 2020, he was awarded a three year Junior Leader Fellowship by the “la Caixa” Foundation.

• • •